minerals

MDPI

Article

Preconcentration and Flotation Recovery of Rare-Earth Minerals from Iron Beneficiation Tailings of the Bayan Obo West Mine

Xinyuan Wu [1,2], Yongli Jin [1,2,3,*], Yan Jia [1,2], Yubao Liu [4], Yu Wei [1,2] and Chiwei Dou [1,2]

[1] School of Rare Earth Industry, Inner Mongolia University of Science and Technology, Baotou 014010, China; xywu266@163.com (X.W.)
[2] National and Local Joint Engineering Research Center of Comprehensive Utilization of Wastes from Mining, Beneficiation, and Smelting of Bayan Obo Associated and Co-Occurring Ores, Baotou 014010, China
[3] Carbon Neutrality Engineering Research Center of Colleges and Universities in Inner Mongolia Autonomous Region, Baotou 014010, China
[4] State Key Laboratory of Bayan Obo Rare Earth Resource Researches and Comprehensive Utilization, Baotou Research Institute of Rare Earths, Baotou 014030, China; liuyubao1985@126.com
* Correspondence: jinyongli731112@126.com; Tel.: +86-138-4721-6326

Abstract

Iron beneficiation tailings from the Bayan Obo West Mine constitute a low-grade secondary rare-earth resource in which rare-earth minerals are finely disseminated and intricately intergrown with gangue. This study quantified the modes of occurrence of rare-earth minerals and assessed an integrated flowsheet comprising screening, magnetic separation, and flotation. The feed contained 1.32 wt.% rare-earth oxides (REOs), as determined by X-ray fluorescence spectrometry (XRF) and inductively coupled plasma optical emission spectrometry (ICP-OES). X-ray diffraction (XRD), scanning electron microscopy coupled with energy-dispersive spectroscopy (SEM-EDS), and automated mineralogy (AMICS) further showed that monazite and bastnäsite hosted 47.39% and 39.19% of the total REOs, respectively. Screening at 74 μm rejected 32.60% of the feed as a coarse fraction containing 0.65 wt.% REOs. Subsequent wet high-intensity magnetic separation reduced the mass entering flotation to 54.35% of the original feed while retaining 74.94% of the feed REOs and increasing the REO grade to 1.82 wt.%. Closed-circuit flotation with one rougher and three cleaner stages yielded a concentrate containing 51.99 wt.% REOs at an overall recovery of 52.38%. Rare-earth minerals accounted for 82.55 wt.% of the concentrate, including 41.65 wt.% monazite and 33.96 wt.% bastnäsite. This study thus demonstrated the feasibility of producing a high-grade rare-earth concentrate from the low-grade, fine-grained iron beneficiation tailings of the Bayan Obo West Mine characterized by complex mineral intergrowths, providing a practical basis for further rare-earth beneficiation and flowsheet optimization.

Keywords: Bayan Obo West Mine; iron beneficiation tailings; rare-earth minerals; process mineralogy; magnetic separation; flotation

Check for updates

Academic Editor: Srecko Stopic

Received: 28 July 2026
Revised: 18 August 2026
Accepted: 25 August 2026
Published: 27 August 2026

Copyright: © 2026 by the authors. Licensee MDPI, Basel, Switzerland. This article is an open access article distributed under the terms and conditions of the Creative Commons Attribution (CC BY) license.

1. Introduction

Rare-earth elements (REEs) have incompletely filled 4f electron shells that impart distinctive magnetic, optical, electrical, and catalytic properties. These properties underpin their use in permanent magnets, catalysts, hydrogen storage materials, electronic devices, new energy equipment, and advanced defense systems [1–3]. Demand for rare earths continues to grow with the global energy transition and the expansion of advanced manufacturing, while high-grade ores that can be readily beneficiated are becoming progressively

depleted. At the same time, efforts to secure critical-metal supplies must be accompanied by environmentally responsible management of tailings storage facilities. Recovering rare earths from tailings, low-grade associated ores, and historically stockpiled solid wastes therefore offers a route to strengthen resource security and improve overall resource utilization [4]. The Bayan Obo deposit is a world-class Fe–REE–Nb polymetallic deposit [5], but long-term production has focused mainly on iron recovery. Because of their fine dissemination, insufficient liberation, and complex intergrowths with carbonates, silicates, fluorite, and iron-bearing minerals, monazite, bastnäsite, and other rare-earth minerals report to the iron beneficiation tailings [6]. These tailings consequently represent both a solid waste management concern and a potentially valuable secondary rare-earth resource.

Secondary rare-earth resources are difficult to beneficiate because of their low grade, fine particle size, complex composition, and limited contrasts in mineral surface properties. Their response to beneficiation depends on the rare-earth mineral assemblage, particle size distribution, degree of liberation, intergrowth texture, gangue assemblage, and reagent regime [7]. Process mineralogy provides the basis for selecting suitable unit operations. Silva et al., for example, showed that mineral tracking, liberation characteristics, and inter-mineral associations are central to the early-stage selection of flotation flowsheets and reagent regimes for REE-bearing minerals [8]. Magnetic separation can serve as a preconcentration step when the target minerals are weakly magnetic. For a low-grade rare-earth ore from the Khalzan Buregtei deposit in Mongolia, Park et al. increased the rare-earth oxide (REO) grade from 7240 to 39,800 mg/kg while maintaining a recovery of approximately 80% [9]. Combined processes can further balance the concentrate grade and recovery. Xiong et al. obtained a concentrate containing 64.75 wt.% REOs at a recovery of 90.81% using a combined flotation–magnetic separation process [10], while Wang et al. recovered xenotime and florencite from silicate minerals by combining magnetic separation and flotation. Flotation selectivity also depends strongly on particle size control and reagent action [11]. In tests on a complex low-grade saprolite rare-earth ore, Abaka-Wood et al. found that appropriate desliming and the use of sodium silicate and starch reduced ultrafine-gangue entrainment and improved selectivity toward rare-earth minerals [12]. From a surface chemistry perspective, Sauber et al. showed that combining oleic acid with alkyl hydroxamate enhanced the hydrophobicity and flotation response of monazite [13]. Studies of Bayan Obo materials have similarly examined preferential and staged recovery. Qin et al. proposed selective reagent regulation for the preferential flotation of rare-earth minerals from iron beneficiation tailings [14]. Wang et al. showed that staged flotation reduced resource losses during the comprehensive recovery of rare earths and fluorite from iron tailings at a Bayan Obo concentrator and improved overall tailings utilization [15]. Fan et al. proposed a direct flotation process as a reference flowsheet for the preferential recovery of rare-earth minerals from Bayan Obo ore [16]. Wang et al. used staged magnetic separation to enrich weakly magnetic rare-earth and niobium minerals from Bayan Obo ore and showed that magnetic property differences are important for the preconcentration of polymetallic tailings [17]. Zhang et al. systematically examined the distribution and flotation behavior of niobium-bearing minerals in Bayan Obo and provided mineralogical and process information for the utilization of complex Nb–REE tailings [18]. Taken together, these studies indicate that flowsheets developed for primary ores should not be assumed to be directly transferable to secondary rare-earth tailings. The role of each beneficiation unit should instead be matched to the rare-earth mineral assemblage, fine particle content, gangue associations, and intergrowth characteristics of the specific tailings.

Compared with the main orebody and East Mine of Bayan Obo, publicly reported studies on the West Mine remain relatively limited, and existing work has focused mainly on the beneficiation of iron-bearing ores and the comprehensive utilization of run-of-mine ore.

Tang and Li primarily investigated the beneficiation behavior of iron-bearing rocks from the Bayan Obo West Mine [19]. Cao and Liu conducted process mineralogy characterization and rare-earth/fluorite flotation tests on West Mine ore; at a grinding fineness of 92.27% passing −0.074 mm, the ore contained 1.78 wt.% REOs, with monazite and bastnäsite contents of 1.80 wt.% and 1.19 wt.%, respectively [20]. These studies show that, in addition to iron resources, the West Mine contains recoverable rare-earth minerals. However, in beneficiation flowsheets dominated by iron recovery, some fine-grained, low-grade, and insufficiently liberated rare-earth minerals fail to report to the iron concentrate and ultimately enter the iron beneficiation tailings. The West Mine iron beneficiation tailings investigated in this study still contained 1.32 wt.% REOs, with monazite and bastnäsite as the principal rare-earth minerals and with fine-grained distribution and complex intergrowths, indicating that the tailings retain further rare-earth recovery potential. At the same time, because the tailings have already undergone upstream iron beneficiation, their mineral composition, particle size distribution, liberation state, and intergrowth relationships differ from those of the run-of-mine ore; therefore, results obtained for the ore cannot be directly used to guide rare-earth beneficiation of the tailings. It is consequently necessary to systematically determine the occurrence and intergrowth characteristics of rare-earth minerals in the West Mine iron beneficiation tailings and to develop an appropriate preconcentration–flotation flowsheet accordingly, thereby improving the comprehensive utilization of associated rare-earth resources in the West Mine.

To address these issues, tailings from the iron beneficiation circuit of a mining company affiliated with Baotou Steel Group in Inner Mongolia, China, were investigated. Their chemical composition, rare-earth mineral assemblage, modes of REO occurrence, particle size distribution, degree of liberation, and mineral associations were characterized. Based on these results, the roles of the individual process units were defined: screening to reject coarse, low-grade material; magnetic separation to preconcentrate weakly magnetic rare-earth minerals and their intergrowths with iron-bearing minerals; and flotation to achieve further upgrading. An integrated flowsheet comprising screening, magnetic separation, and closed-circuit flotation with one rougher and three cleaner stages was then developed. The study examined the factors limiting the beneficiation of low-grade rare earths in the Bayan Obo West Mine iron beneficiation tailings and evaluated the effects of feed mass reduction by screening and magnetic preconcentration on the flotation load and concentrate production. The results are intended to provide a mineralogical basis and process guidance for further rare-earth beneficiation and flowsheet optimization of the Bayan Obo West Mine iron beneficiation tailings.

2. Materials and Methods

2.1. Experimental Materials

The test material was collected beginning on 20 January 2026 from the tailings stream of an iron beneficiation circuit operated by a mining company affiliated with Baotou Steel in Baotou, Inner Mongolia, China. Increment samples were collected by intercepting the entire tailings stream at 30 min intervals for 10 consecutive days, yielding approximately 500 kg of composite bulk sample. Following homogenization, air drying, and sample splitting, subsamples were prepared for chemical analysis, mineralogical characterization, particle size analysis, magnetic separation tests, and flotation tests. To ensure comparability across the analytical measurements and beneficiation tests, all subsamples were derived from the same homogenized bulk sample. The major mineral phases were identified using an X-ray diffractometer (XRD, SmartLab 9 kW, Rigaku Corporation, Tokyo, Japan). Major oxides and multielement compositions were analyzed using an X-ray fluorescence spectrometer (XRF, S8 TIGER, Bruker AXS GmbH, Karlsruhe, Germany), and REOs and related elemental

contents were determined using an inductively coupled plasma optical emission spectrometer (5110 ICP-OES, Agilent Technologies Inc., Santa Clara, CA, USA). A scanning electron microscope (SEM, ZEISS SUPRA55, Carl Zeiss AG, Oberkochen, Germany) equipped with an energy-dispersive spectroscopy system (EDS, QUANTAX 400, Bruker AXS GmbH, Karlsruhe, Germany) was used to examine the morphology, dissemination characteristics, and elemental composition of the rare-earth minerals. An AMICS automated mineralogy system (Bruker AXS GmbH, Karlsruhe, Germany) was used to determine mineral composition, particle size distribution, degree of liberation, and mineral associations based on BSE imaging and EDS analysis. Standard sieves with apertures of 150, 74, 45, 38, and 25 μm were used for particle size analysis. Three reagents were used in the flotation tests: sodium silicate, GF-1, and FM-132. Commercial sodium silicate had a modulus of 2.7, corresponding to a SiO_2/Na_2O molar ratio of 2.7, and was prepared as a 4 wt.% aqueous solution. GF-1 was an industrial-grade hydroxamate rare-earth collector, whereas FM-132 was an industrial-grade mixed-alcohol frother; the exact compositions and component ratios of these proprietary formulations were not disclosed by the suppliers. Reagent dosages are reported per ton of dry feed. Laboratory tap water was used throughout the tests.

2.2. Experimental Method

2.2.1. Tailings Preconcentration

Screening was first performed using a CTS510 electromagnetic vibrating mesh digitally controlled high-frequency screen (Tangshan Haipu Technology Co., Ltd., Tangshan, China) with a nominal aperture of 74 μm, commonly designated as 200 mesh. The low-grade +74 μm oversize was rejected as coarse tailings to reduce the mass treated in subsequent operations.

The −74 μm undersize was used as the magnetic separation feed. Preconcentration was performed using an LGS-EX vertical ring induction wet high-intensity magnetic separator (Longi Magnet Co., Ltd., Shenyang, China). This step exploited the differences in magnetic properties among weakly magnetic rare-earth minerals, their intergrowths with iron-bearing minerals, and nonmagnetic carbonate and silicate gangue. The effects of the magnetic flux density, pulp solids concentration, and feed velocity on the REO grade and recovery were evaluated, and the resulting magnetic concentrate was used as the flotation feed. Magnetic separation tests were conducted over magnetic flux densities of 0.6–1.4 T, pulp solids concentrations of 5–25 wt.%, and feed velocities of 0.5–2.5 m/s.

2.2.2. Flotation

Flotation tests were conducted in an XFD-IV flotation machine (Jilin Prospecting Machinery Factory, Changchun, China) using 0.75, 0.50, 0.25, and 0.15 L cells selected according to the mass yield at each stage. The impeller speed and aeration conditions were kept constant in all flotation tests, with an air flow rate of 0.10 m^3/h (1.67 L/min) and an impeller speed of 1992 rpm. Sodium silicate, GF-1, and FM-132 were added sequentially, and the froth was collected after the specified conditioning period. Following the addition of each reagent, the pulp was conditioned for 5 min before froth collection for the specified flotation time. After sodium silicate addition and conditioning, the pulp pH, measured using a pHs-3C pH meter, stabilized at 8.0–9.0. Roughing mainly recovered liberated and partially intergrown rare-earth minerals, whereas three successive cleaner stages progressively removed carbonate, silicate, fluorite, and apatite gangue to improve separation between the rare-earth and gangue minerals. In the rougher flotation condition tests, the sodium silicate dosage ranged from 1.33 to 3.11 kg/t, the GF-1 dosage from 0.67 to 1.56 kg/t, the temperature from 20 to 60 °C, and the flotation time from 60 to 180 s. Zhao et al. [21] reported that, in rare-earth flotation tests on Bayan Obo tailings, REO

recovery generally increased with a pulp solids concentration over the range of 20–60 wt.%. To obtain higher REO recovery and further examine the variation in grade and recovery at high pulp densities, the rougher pulp solids concentration in this study was set at 50–70 wt.%. The REO recovery of each product was calculated from its mass and REO grade using Equation (1).

$$\varepsilon_c(\%) = \frac{Q_c \cdot \beta_c}{Q_0 \cdot \beta_0} \times 100\% \quad (1)$$

In Equation (1), ε_c denotes the concentrate recovery. Q_c and Q_0 denote the masses of the concentrate and feed, respectively, and β_c and β_0 denote the corresponding REO grades.

Each experimental condition was evaluated in at least three replicate tests. The reproducibility results in Tables 5–7 are reported as mean ± standard deviation (SD), and the relative standard deviation (RSD) was used to assess test repeatability. Across the magnetic separation, rougher flotation, and open-circuit cleaning replicate tests, the RSD values of the concentrate REO grade and recovery were all below 2.7%, indicating good repeatability. Mass yield and REO recovery were calculated from the measured masses and chemical analysis results, and the calculated values were reported to two decimal places to ensure consistency in the mass and metallurgical balance calculations.

3. Results

3.1. Mineralogical Characterization of the Bayan Obo West Mine Iron Beneficiation Tailings

3.1.1. Chemical Composition

Table 1 summarizes the multielement chemical composition of the Bayan Obo West Mine iron beneficiation tailings. With an REO content of 1.32 wt.%, the material represented a low-grade secondary rare-earth resource. The total iron (TFe) content was 9.95 wt.%, whereas the magnetic iron (mFe) content was only 1.20 wt.%. This difference indicated that most strongly magnetic iron minerals amenable to low-intensity magnetic separation had already been removed during upstream iron beneficiation. The CaO, MgO, and SiO_2 contents were 22.23 wt.%, 14.31 wt.%, and 16.46 wt.%, respectively, confirming that carbonate and silicate minerals dominated the gangue assemblage. The sample also contained 462 mg/kg Sc_2O_3, indicating the potential for broader multielement utilization, although the present study focused on rare-earth recovery. F-REO denotes the rare-earth oxide content hosted by the bastnäsite phase, whereas P-REO denotes the rare-earth oxide content hosted by the monazite phase; these parameters distinguish the principal fluorocarbonate-type and phosphate-type rare-earth phases.

Table 1. Multielement chemical composition of the West Mine iron beneficiation tailings. Major components are reported in wt.%, and Sc_2O_3 is reported in mg/kg.

Name	TFe	mFe	CaO	MgO	SiO_2	Al_2O_3	P	K_2O	Na_2O
Content	9.95	1.2	22.23	14.31	16.46	2.48	0.52	2.13	1.02
Name	REO	F-REO	P-REO	Nb_2O_5	BaO	Sc_2O_3(mg/kg)	CaF_2	MnO	ThO_2
Content	1.32	0.57	0.75	0.094	0.98	462	4.40	2.45	0.049

3.1.2. Mineral Composition and Modes of Rare-Earth Occurrence

The major mineral phases were identified by XRD, whereas AMICS was used to quantify the mineral contents and characterize the mineral distributions and associations. The results are presented in Figures 1 and 2.

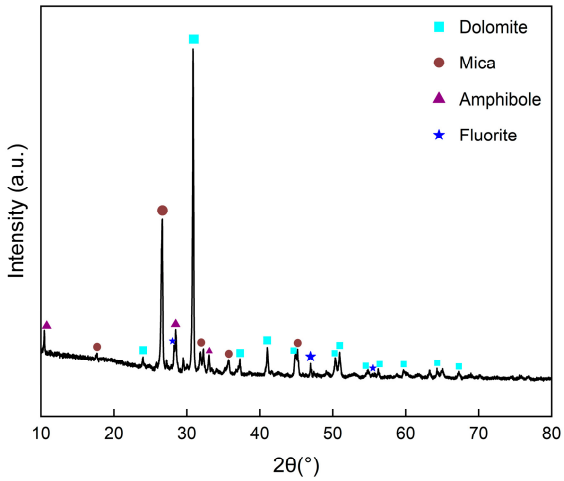


Figure 1. XRD pattern of the Bayan Obo West Mine iron beneficiation tailings.

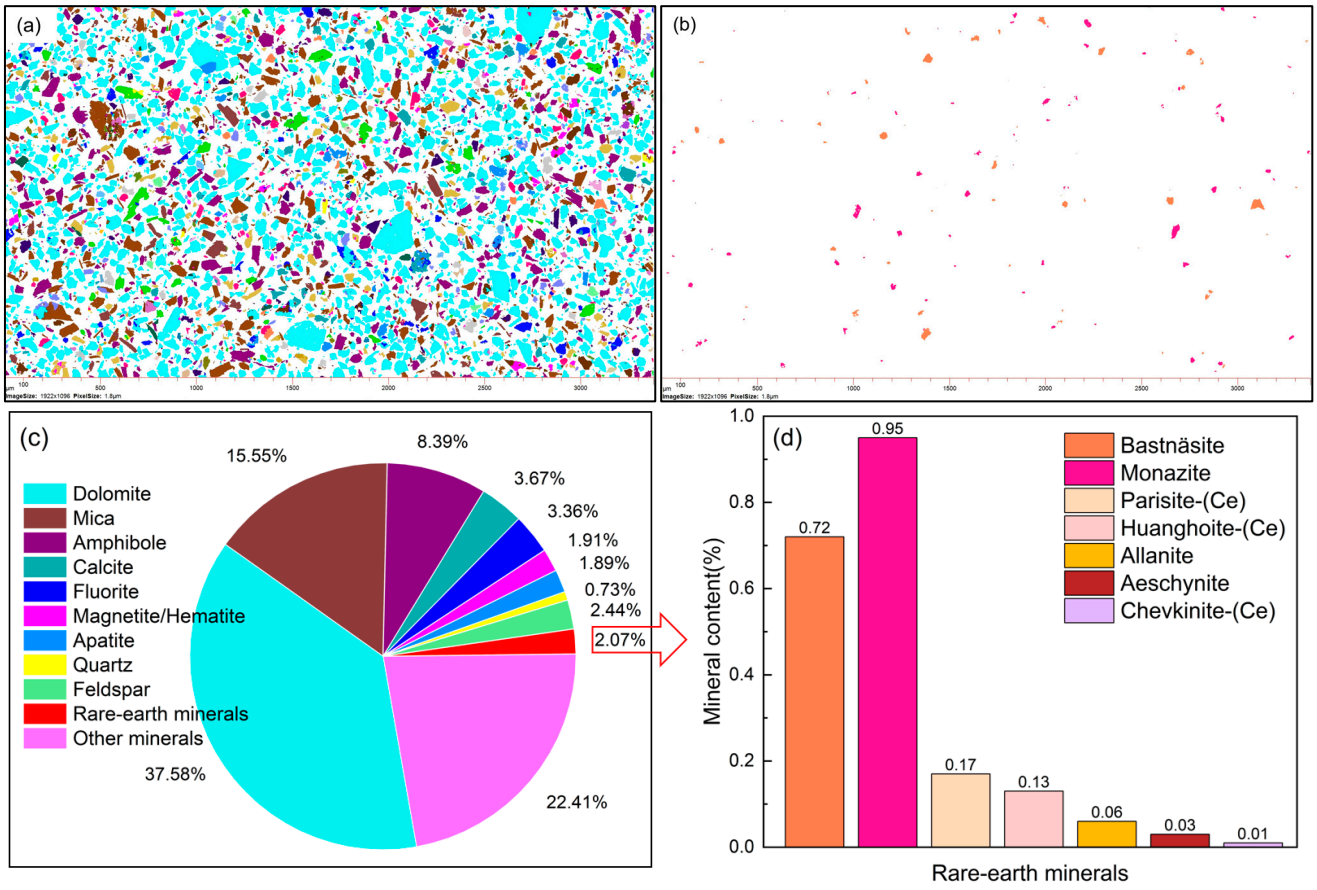


Figure 2. Mineralogical characterization of the West Mine iron beneficiation tailings: (**a**) AMICS mineral map of all phases; (**b**) AMICS rare-earth mineral map; (**c**) major mineral composition; and (**d**) rare-earth mineral composition.

The XRD pattern in Figure 1 shows that the sample was dominated by carbonate and silicate minerals, principally dolomite, mica, amphibole, and calcite. Figure 2a–d provide the qualitative and quantitative mineralogical characteristics of the sample. Figure 2a presents the complete mineral-phase classification corresponding to the backscattered electron image acquired by AMICS, with colors corresponding to the mineral phases listed in the legends of Figure 2c,d. Dolomite was the most widely distributed mineral and formed the principal matrix. Mica generally occurred as platy or flaky grains,

whereas amphibole occurred as prismatic or irregular granular particles accompanied by calcite, feldspar, pyroxene, fluorite, and other gangue minerals. Dolomite, mica, and amphibole therefore constituted the principal gangue assemblage and the main minerals requiring depression during flotation. Figure 2b isolates the rare-earth phases from the complete mineral classification, including bastnäsite, monazite, parisite-(Ce), huanghoite-(Ce), aeschynite, allanite, chevkinite-(Ce), and other rare-earth minerals. These minerals occurred at low contents and were spatially dispersed, mainly as spot-like particles, short laths, and irregular fine grains, with only limited local clustering, reflecting a low-content, finely disseminated rare-earth mineral assemblage. Comparison of Figure 2a,b further showed that monazite occurred both as discrete granular, blocky, or elliptical particles and as multiphase intergrowths with dolomite, mica, and iron-bearing minerals. The quantitative results in Figure 2c showed that dolomite and mica accounted for 37.58 wt.% and 15.55 wt.% of the sample, respectively. Amphibole, calcite, and fluorite accounted for 8.39 wt.%, 3.67 wt.%, and 3.36 wt.%, respectively, whereas other minerals accounted for 22.41 wt.%. These proportions further confirmed the predominance of carbonate and silicate gangue. Feldspar and apatite accounted for 2.44 wt.% and 1.89 wt.%, respectively. Although present at relatively low contents, both minerals have floatabilities similar to those of rare-earth minerals and may therefore undergo nonselective recovery during flotation. The quantitative results in Figure 2d showed that rare-earth minerals accounted for 2.07 wt.% of the sample. Monazite ($(Ce,La,Nd)PO_4$) and bastnäsite ($(Ce,La)CO_3F$) were the principal rare-earth minerals, with contents of 0.95 wt.% and 0.72 wt.%, respectively. Parisite-(Ce) ($Ca(Ce,La)_2(CO_3)_3F_2$), huanghoite-(Ce) ($Ba_2(Ce,La)(CO_3)_3F$), allanite ($(Ca,Ce)_2(Al,Fe)_3(SiO_4)_3(OH)$), aeschynite ($(Ce,La)(Ti,Nb)_2O_6$), and chevkinite-(Ce) ($(Ce,La,Ca)_4(Fe,Mg)_2(Ti,Fe)_3Si_4O_{22}$) each accounted for less than 0.20 wt.%. Thus, although the rare-earth minerals were present at low contents and were finely disseminated, most REOs occurred in discrete rare-earth mineral phases, providing a mineralogical basis for recovery by physical beneficiation.

The distribution of REOs among the mineral phases was calculated from the rare-earth mineral composition shown in Figure 2d, the REO contents of the individual minerals [5], and the elemental balance. The results are listed in Table 2.

Table 2. Distribution of rare-earth oxides among the mineral phases.

Mineral	Bastnäsite	Monazite	Parisite-(Ce)	Huanghoite-(Ce)	Aeschynite	Allanite	Chevkinite-(Ce)	Other Minerals	Total
Mineral content (wt.%)	0.72	0.95	0.17	0.13	0.03	0.06	0.01	97.93	100
REO content (wt.%)	71.83	65.83	57.81	36.26	33.27	22.05	44.86	0.004	1.32
REO distribution (%)	39.19	47.39	7.45	3.57	0.76	1.00	0.34	0.3	100

Monazite and bastnäsite hosted 47.39% and 39.19% of the total REOs, respectively, and together contributed 86.58%. When parisite-(Ce), huanghoite-(Ce), aeschynite, allanite, and chevkinite-(Ce) were included, more than 99.7% of the REOs occurred in discrete rare-earth minerals, whereas only approximately 0.3% was dispersed in other minerals. The rare earths in the West Mine iron beneficiation tailings were therefore not predominantly present as lattice-bound substitutions. This mode of occurrence supports their recovery through mineral liberation followed by interfacial separation.

Standard sieves with apertures of 150, 74, 45, 38, and 25 μm were used to determine the particle size composition of the tailings and the distribution of REOs among the size frac-

tions. AMICS was additionally used to determine the cumulative particle size distributions of the principal rare-earth minerals. Table 3 and Figure 3 present the results.

Table 3. Particle size composition and REO distribution of the West Mine iron beneficiation tailings.

Particle Size Fraction (μm)	Mass Yield (%)	Cumulative Undersize Yield (%)	REO Grade (wt.%)	REO Distribution (%)
+150	15.02	100	0.76	9.06
−150 +74	14.50	84.98	0.89	10.24
−74 +45	16.25	70.48	1.27	16.37
−45 +38	4.84	54.23	1.35	5.18
−38 +25	8.13	49.39	1.46	9.41
−25	41.26	41.26	1.52	49.74
Total	100	-	1.26	100

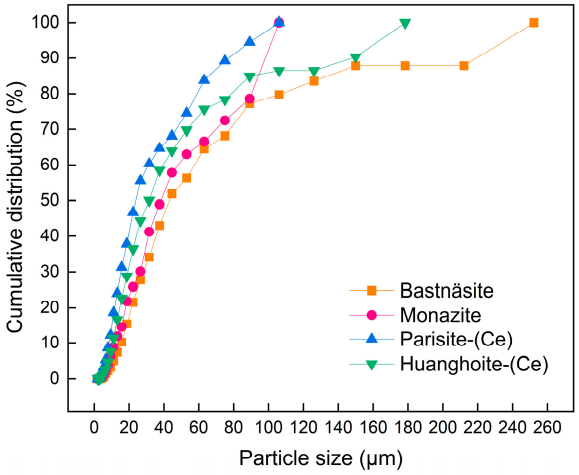


Figure 3. Cumulative particle size distributions of the principal rare-earth minerals.

Table 3 and Figure 3 show a preferential distribution of REOs in the fine fractions. The −25 μm fraction accounted for 41.26% of the feed mass but contained 49.74% of the total REOs, at a grade of 1.52 wt.%. The combined −74 μm fractions represented 70.48% of the mass and contained 80.70% of the total REOs. By contrast, the +74 μm coarse fraction accounted for 29.52% of the mass but only 19.30% of the total REOs. The +150 μm and −150 + 74 μm fractions had REO grades of 0.76 wt.% and 0.89 wt.%, respectively, both substantially below the feed grade. The cumulative distributions in Figure 3 further showed that monazite, bastnäsite, parisite-(Ce), and huanghoite-(Ce) occurred predominantly below 100 μm. The low REO grades of the coarse fractions therefore created an opportunity for upstream waste rejection and a corresponding reduction in the mass treated in subsequent operations. The independently measured whole-feed REO grade was 1.32 wt.%, compared with a size-by-size weighted value of 1.26 wt.%. The small difference was attributed to sampling variability, and 1.32 wt.% was used as the feed grade in all subsequent recovery calculations.

SEM-EDS and AMICS were subsequently used to characterize the dissemination textures, degrees of liberation, and mineral associations of the principal rare-earth minerals. The results are presented in Figure 4 and Table 4.

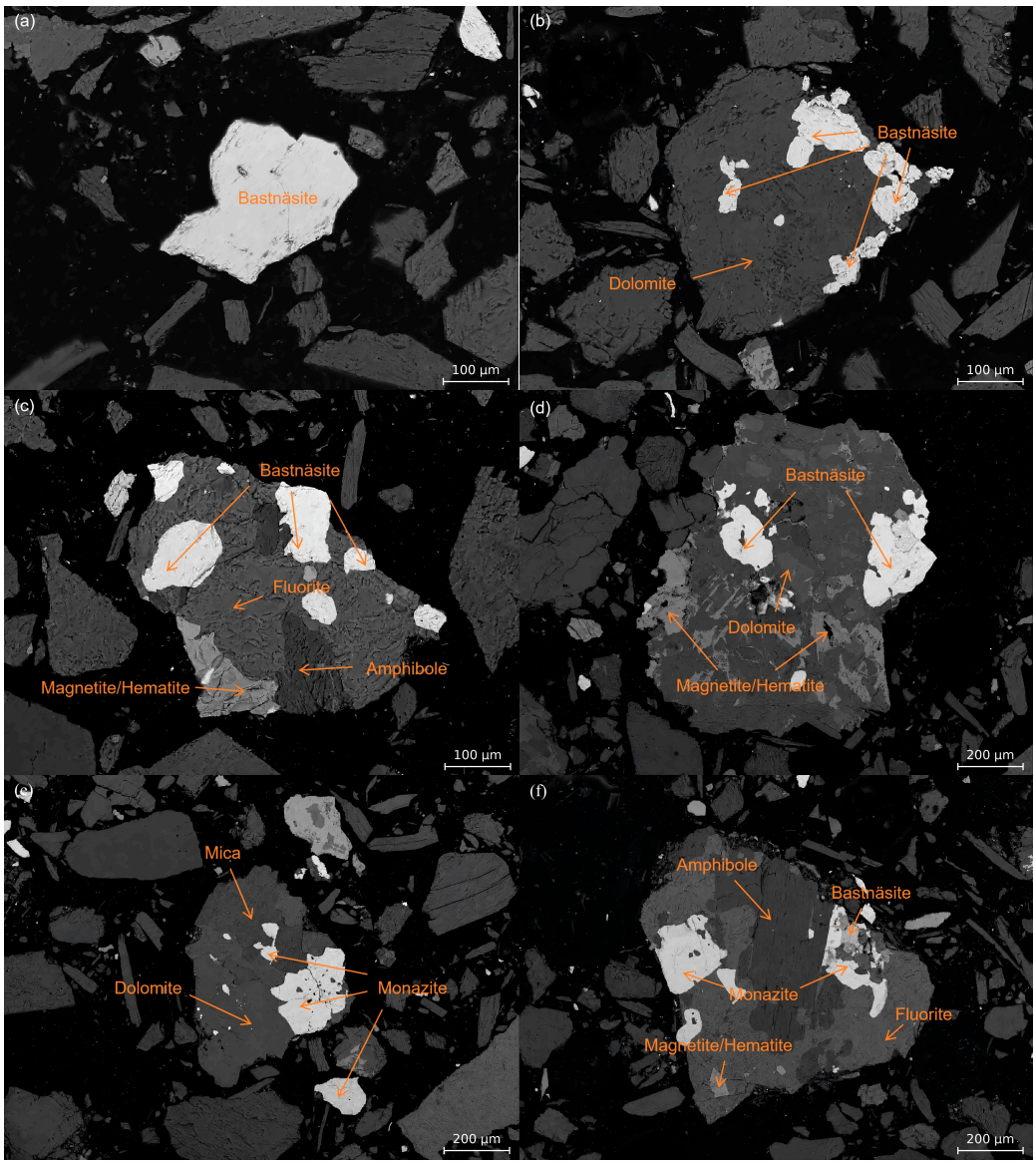


Figure 4. Representative dissemination and intergrowth characteristics of bastnäsite and monazite: (**a**) liberated bastnäsite; (**b**) bastnäsite disseminated along the margins of dolomite; (**c**) bastnäsite intergrown with dolomite and amphibole; (**d**) bastnäsite intergrown with dolomite and magnetite/hematite; (**e**) monazite intergrown with dolomite and mica; and (**f**) monazite and bastnäsite intergrown with amphibole, fluorite, and magnetite/hematite.

Table 4. Liberation and mineral association proportions of the principal rare-earth minerals.

Mineral	Degree of Liberation (%)	Mineral Association (%)						
		Carbonates	Silicates	Fe-Bearing	Fluorite	Apatite	Barite	Other Minerals
Bastnäsite	48.43	24.07	10.01	4.81	7.42	0.36	1.17	3.73
Monazite	65.09	14.97	9.58	3.86	2.45	0.67	0.49	2.89
Parisite-(Ce)	20.9	34.17	16.65	11.02	6.40	1.60	5.00	4.26
Huanghoite-(Ce)	27.49	36.32	10.51	7.36	5.15	0.87	6.43	5.87

Figure 4 and Table 4 showed that monazite had a degree of liberation of 65.09%, compared with 48.43% for bastnäsite. Figure 4a shows a relatively intact, blocky liberated grain of bastnäsite, whereas Figure 4e shows granular liberated or nearly liberated particles of monazite. These liberated particles constituted the fraction most directly recoverable by flotation. However, substantial proportions of the rare-earth minerals remained in

edge-adjacent, interlocked, or multiphase composite particles. Bastnäsite was associated with carbonate minerals, silicate minerals, and fluorite at proportions of 24.07%, 10.01%, and 7.42%, respectively. Fine bastnäsite occurred discontinuously along the dolomite margins in Figure 4b and formed composite particles with dolomite, amphibole, fluorite, and magnetite/hematite in Figure 4c,d. During flotation, these intergrowths could either report to the froth together with carbonate, silicate, and fluorite gangue, thereby lowering the concentrate quality, or remain insufficiently liberated and be lost to the tailings, thereby limiting bastnäsite recovery. Although monazite was more highly liberated than bastnäsite, 14.97% and 9.58% of the monazite remained associated with carbonate and silicate minerals, respectively. The intergrowths of monazite with dolomite, mica, and iron-bearing minerals in Figure 4e,f further confirmed incomplete liberation. Parisite-(Ce) and huanghoite-(Ce) had degrees of liberation of only 20.90% and 27.49%, respectively, and carbonate mineral association proportions of 34.17% and 36.32%. These subordinate rare-earth minerals therefore occurred mainly as fine composite particles and were particularly susceptible to loss or gangue carryover during cleaning. The difficult beneficiation response of the West Mine iron beneficiation tailings was consequently governed not only by the low REO grade but also by the complex intergrowth of fine rare-earth minerals with carbonates, silicates, fluorite, apatite, and iron-bearing minerals. The downstream flowsheet was therefore structured to remove low-grade coarse particles and nonmagnetic gangue by screening and magnetic separation before flotation reagents were used to enhance the differences in floatability between the rare-earth minerals and the principal gangue phases.

3.2. Preconcentration of the Tailings

3.2.1. Tailings Rejection by Screening

On the basis of the particle size–grade relationship in Table 3 and the intergrowth characteristics shown in Figure 4 and Table 4, screening at 74 μm was selected as the first feed mass reduction step in the overall flowsheet. This stage was not intended to produce a rare-earth concentrate directly. Its function was to reject coarse gangue with a low REO grade and a limited contribution to rare-earth recovery, thereby reducing the material load on the subsequent magnetic separation and flotation stages. Figure 5 presents the mass and metallurgical balance for the screening test.

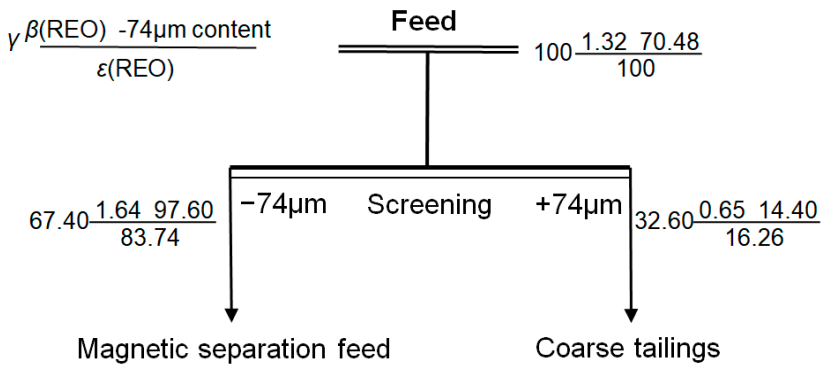


Figure 5. Mass and metallurgical balance for the 74 μm screening test. Here, γ denotes mass yield (%), β(REO) denotes REO grade (wt.%), ε(REO) denotes REO recovery (%), and the final value shown for each stream denotes the −74 μm content (%).

The +74 μm oversize obtained by screening had a mass yield of 32.60%, an REO grade of 0.65 wt.%, and an REO recovery of 16.26%, and was therefore rejected as a low-grade coarse fraction. The −74 μm undersize accounted for 67.40% of the mass. Its REO grade increased from 1.32 wt.% to 1.64 wt.%, its −74 μm content increased to 97.60%, and it retained 83.74% of the total REOs. Screening therefore rejected approximately one-third of

the low-grade coarse material and reduced the downstream feed mass without introducing an additional grinding stage. The +74 μm mass fraction measured by laboratory sieve analysis was 29.52%, whereas the oversize yield obtained in the high-frequency screening test was 32.60%. This difference was attributed to the different screening modes, the partitioning of near-size particles, and sampling variability.

3.2.2. Preconcentration by Magnetic Separation

The −74 μm undersize was used as the magnetic separation feed. Previous studies on Bayan Obo ores have shown that monazite and bastnäsite are weakly magnetic minerals, with specific magnetic susceptibilities of approximately 12.6×10^{-6} and 11.4×10^{-6} cm^3/g, respectively; those of fluorite, quartz, and calcite are still lower, at approximately 4.2×10^{-6}, 3.5×10^{-6}, and 1.4×10^{-6} cm^3/g, respectively, while dolomite, Fe-bearing mica, and amphibole also exhibit different degrees of weak magnetic response [17]. Because the feed in this study had already undergone upstream iron beneficiation, most strongly magnetic iron minerals had been removed. In addition to liberated particles, the remaining rare-earth minerals also occurred as intergrowths with magnetite/hematite, Fe-bearing mica, amphibole, and other minerals (Figure 4 and Table 4). Dolomite, calcite, quartz, feldspar, and fluorite generally have low magnetic susceptibilities, whereas residual iron oxides and Fe-rich minerals such as Fe-bearing mica and amphibole have higher susceptibilities. High-gradient magnetic separation partitioned the feed on the basis of these differences: weakly magnetic rare-earth minerals and their intergrowths with iron-bearing minerals preferentially reported to the magnetic product, while part of the weakly responsive or nearly nonmagnetic carbonate and silicate gangue was rejected. The objective of this stage was not to produce the final rare-earth concentrate, but to reduce the feed mass before flotation, increase the REO grade, and stabilize the feed composition. The effects of the magnetic flux density, pulp solids concentration, and feed velocity on the concentrate grade and recovery were evaluated over ranges of 0.6–1.4 T, 5–25 wt.%, and 0.5–2.5 m/s, respectively. Figure 6 presents the condition test results, and Table 5 summarizes the reproducibility test results.

Table 5. Reproducibility test results for magnetic separation.

Test No.	Product	Mass Yield (%)	REO Grade (wt.%)	REO Recovery (%)
1	Concentrate	79.60	1.85	91.01
	Tailings	20.40	0.71	8.99
	Feed	100	1.62	100
2	Concentrate	80.87	1.82	89.05
	Tailings	19.13	0.94	10.95
	Feed	100	1.65	100
3	Concentrate	81.45	1.79	88.41
	Tailings	18.55	1.03	11.59
	Feed	100	1.65	100
Mean	Concentrate	80.64 ± 0.95	1.82 ± 0.03	89.49 ± 1.35
	Tailings	19.36 ± 0.95	0.89 ± 0.17	10.51 ± 1.35
	Feed	100	1.64 ± 0.02	100

Figure 6a illustrates the trade-off between magnetic force and separation selectivity. Increasing the magnetic flux density from 0.6 to 1.2 T strengthened the magnetic forces acting on weakly magnetic rare-earth minerals, intergrowths with iron-bearing minerals, and fine rare-earth composite particles attached to mineral surfaces. Their probability of capture consequently increased, and REO recovery rose from 73.06% to 89.45%. At 1.4 T,

however, low-susceptibility, low-grade intergrowths, iron-bearing mica and amphibole, and composite particles containing carbonate and silicate gangue were also captured. Recovery continued to increase, but the concentrate REO grade decreased to 1.74 wt.%, indicating a loss of selectivity. A magnetic flux density of 1.2 T was therefore selected to balance target particle capture against gangue rejection. Figure 6b shows that increasing the pulp solids concentration from 5 to 15 wt.% increased both the number of target particles entering the effective magnetic field zone per unit time and the probability of contact between weakly magnetic rare-earth minerals or iron-bearing intergrowths and the magnetic matrix, which improved recovery. Above 15 wt.%, increased pulp viscosity, particle crowding, and nonselective entrainment reduced both grade and recovery. A pulp solids concentration of 15 wt.% therefore balanced magnetic capture efficiency and pulp fluidity. Figure 6c shows that increasing the feed velocity from 0.5 to 2.5 m/s shortened the particle residence time in the magnetic field and increased hydrodynamic drag. Fine rare-earth minerals with low magnetic susceptibility and intergrowths with low iron contents were preferentially lost to the tailings, whereas the retained particles generally had higher magnetic susceptibility or a larger iron-bearing component. Consequently, the concentrate grade increased as the recovery decreased. A feed velocity of 1.5 m/s was selected before the pronounced decline in recovery. At this velocity, the concentrate contained 1.84 wt.% REOs at a stage recovery of 89.45%. Considering the three variables together, the selected magnetic separation conditions were a magnetic flux density of 1.2 T, a pulp solids concentration of 15 wt.%, and a feed velocity of 1.5 m/s. Under these conditions, the principal process benefit was a substantial reduction in downstream feed mass and reagent demand, accompanied by a comparatively modest increase in grade.

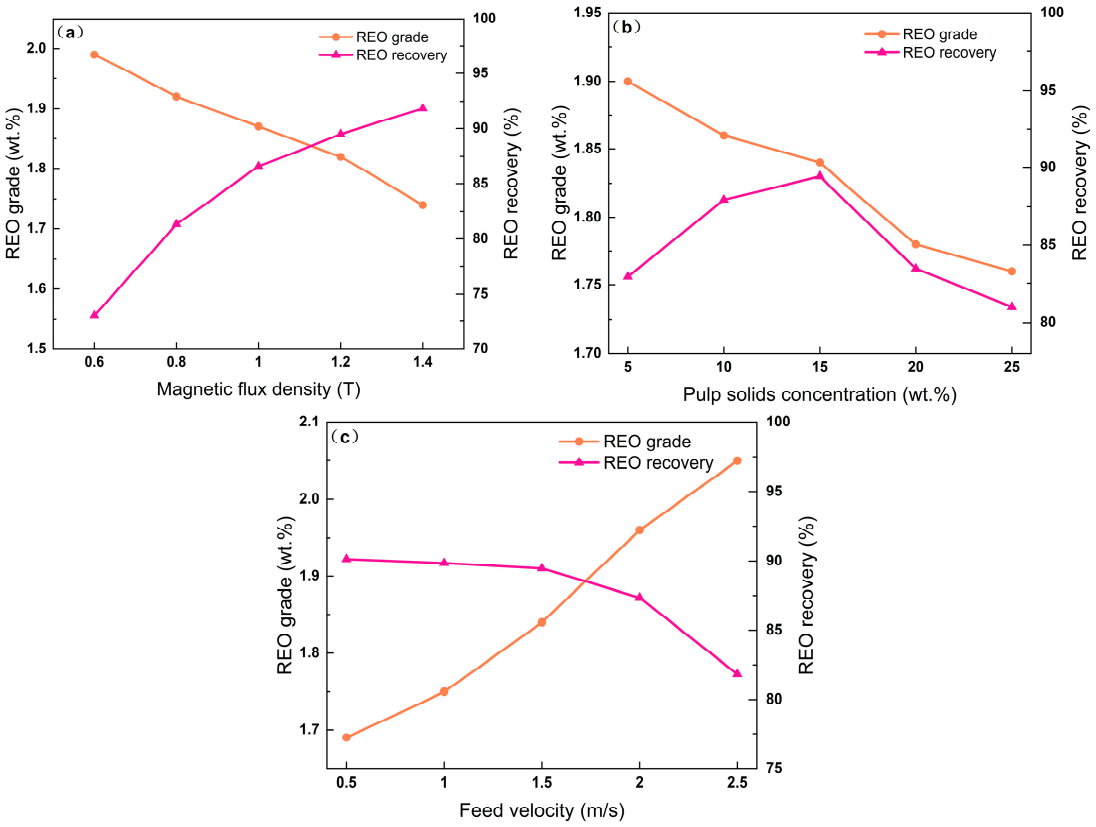


Figure 6. Effects of magnetic separation conditions on the REO grade and recovery of the concentrate: (**a**) magnetic flux density; (**b**) pulp solids concentration; and (**c**) feed velocity.

Across the three replicate tests, the magnetic concentrate had a mass yield of 80.64 ± 0.95%, an REO grade of 1.82 ± 0.03 wt.%, and a stage recovery of 89.49 ± 1.35%. The small standard deviations indicate good repeatability of the magnetic separation tests. The magnetic tailings had a mean REO grade of 0.89 wt.%, substantially lower than those of the feed and concentrate.

Figure 7 presents the combined screening–magnetic separation flowsheet.

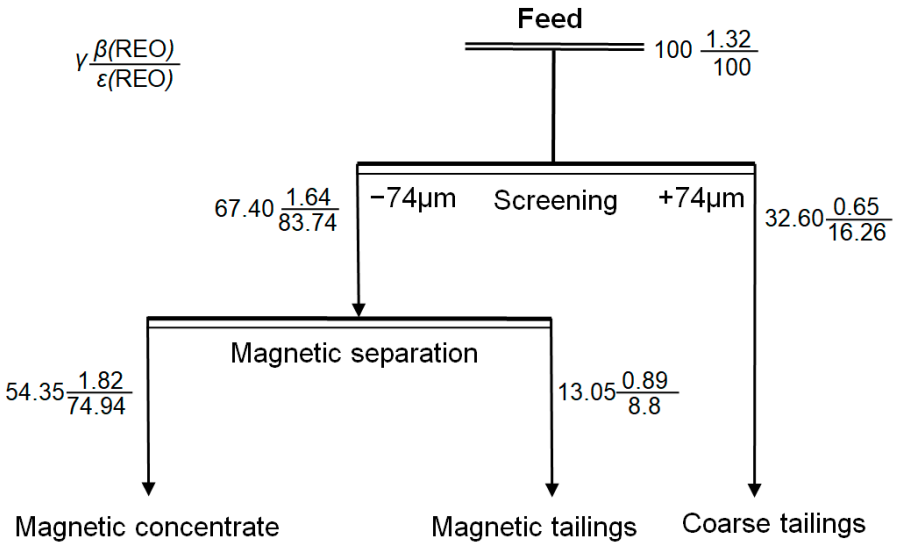


Figure 7. Mass and metallurgical balance for the combined screening and magnetic separation tests.

After screening and magnetic separation, the magnetic concentrate represented 54.35% of the original feed mass, contained 1.82 wt.% REOs, and retained 74.94% of the REOs in the original feed. The mass yields of the screening coarse tailings and magnetic tailings were 32.60% and 13.05%, respectively, corresponding to a combined rejection of 45.65% of the original feed. Thus, the mass entering flotation was reduced from 100% to 54.35% of the original feed, while the REO grade increased from 1.32 wt.% to 1.82 wt.%, an increase of 37.9%. The principal advantage of this pretreatment was not to pursue a high enrichment ratio, but to reject screening and magnetic separation tailings with a combined mass yield of 45.65% while retaining approximately three-quarters of the feed REOs, thereby reducing the downstream flotation load.

3.3. Intensive Upgrading by Flotation

The magnetic concentrate was used as the flotation feed. Because it contained substantial proportions of dolomite, mica, and amphibole, a 4 wt.% sodium silicate solution was used to depress carbonate and silicate gangue. A 2 wt.% GF-1 solution served as the collector for the rare-earth minerals, and FM-132 served as the frother. The evaluated flotation flowsheet comprised one rougher and three cleaner stages. Roughing preferentially recovered the more readily floatable monazite and bastnäsite, whereas successive cleaning progressively rejected carbonate, silicate, and other gangue minerals. Reproducibility was assessed using three magnetic separation replicates, five rougher flotation replicates, and three open-circuit cleaning replicates. The corresponding mean values are reported below.

Figure 8 summarizes the effects of the rougher flotation conditions on the concentrate REO grade and recovery.

Figure 8a shows that increasing the sodium silicate dosage from 1.33 to 2.22 kg/t raised the REO grade of the rougher concentrate from 5.03 wt.% to 7.20 wt.%, while recovery remained at 92.01%. This response was consistent with the adsorption of silicate species on carbonate and other gangue surfaces, which increases surface hydration and dispersion

and thereby suppresses gangue flotation and slime coating. Sodium silicate adsorption is mineral-dependent, however, and Ca-bearing surface sites may form hydrophilic silicate-containing species that hinder hydroxamate adsorption [22]. The sharp decreases in both grade and recovery at higher sodium silicate dosages therefore suggested over-depression of rare-earth minerals and their intergrowths, potentially enhanced by dissolved Ca^{2+} in the pulp [23]. Figure 8b shows that increasing the GF-1 dosage from 0.67 to 1.11 kg/t increased recovery from 43.03% to 92.01%. Hydroxamate collectors generally interact with exposed metal sites through oxygen donor groups, while the ligand structure and interfacial hydration affect the adsorption selectivity between bastnäsite and carbonate gangue [23,24]. The increase in recovery was therefore consistent with greater collector coverage of monazite and bastnäsite. Above 1.11 kg/t, recovery reached a plateau while grade declined, which may reflect less-selective adsorption on Ca/Mg-bearing gangue, greater froth stability, and increased mechanical carryover of fine particles.

Figure 8c shows that increasing the temperature from 20 to 50 °C raised the concentrate grade to approximately 7.77 wt.%. When the temperature reached 60 °C, recovery increased to 92.01%, but the grade decreased to 7.20 wt.%. The higher recovery may have resulted from faster conditioning and flotation kinetics, whereas the decrease in grade indicates that the higher temperature also promoted the recovery of weakly floatable intergrowths or gangue. Therefore, 60 °C was selected as the optimum rare-earth flotation temperature under the present test conditions. This temperature is consistent with that used for rare-earth flotation in Reference [21], and the variation trends in rare-earth recovery and grade were similar to those reported in Reference [25]. Figure 8d shows that the concentrate grade reached a maximum of 7.37 wt.% at 55 wt.% solids, whereas recovery continued to increase with the pulp solids concentration. At 60 wt.% solids, recovery increased markedly while the grade remained relatively high. Above 60 wt.%, the pronounced grade decline was likely associated with particle crowding, altered froth drainage, and increased water recovery. Because water recovery is a major driver of fine gangue entrainment and is sensitive to flotation hydrodynamics [26], a pulp solids concentration of 60 wt.% was selected as the practical balance between grade and recovery.

Figure 8e shows that extending the flotation time from 60 to 180 s continuously increased recovery but reduced the concentrate grade from approximately 8.4 wt.% to approximately 6.6 wt.%. The early flotation period likely favored liberated rare-earth minerals with more complete collector coverage. As flotation proceeded, slow-floating intergrowths and fine gangue were increasingly recovered through both true flotation and entrainment. Time-resolved batch flotation studies have similarly shown that froth properties and entrainment change with the flotation time and pulp density [27]. A flotation time of 150 s was therefore selected because the subsequent recovery gain was marginal relative to the additional gangue recovery. At 150 s, the concentrate contained 7.20 wt.% REOs at a recovery of 92.01%.

The selected rougher flotation conditions were 2.22 kg/t sodium silicate, 1.11 kg/t GF-1, 0.04 kg/t FM-132, a pulp solids concentration of 60 wt.%, a temperature of 60 °C, and a flotation time of 150 s. The sequence of one rougher followed by three cleaner stages separated the two process objectives. Roughing maximized the recovery of liberated and partially intergrown rare-earth minerals, whereas successive cleaning increased the concentrate grade by progressively removing carbonate, silicate, and fluorite gangue.

Five replicate tests were conducted under the selected rougher flotation conditions. The results are presented in Table 6.

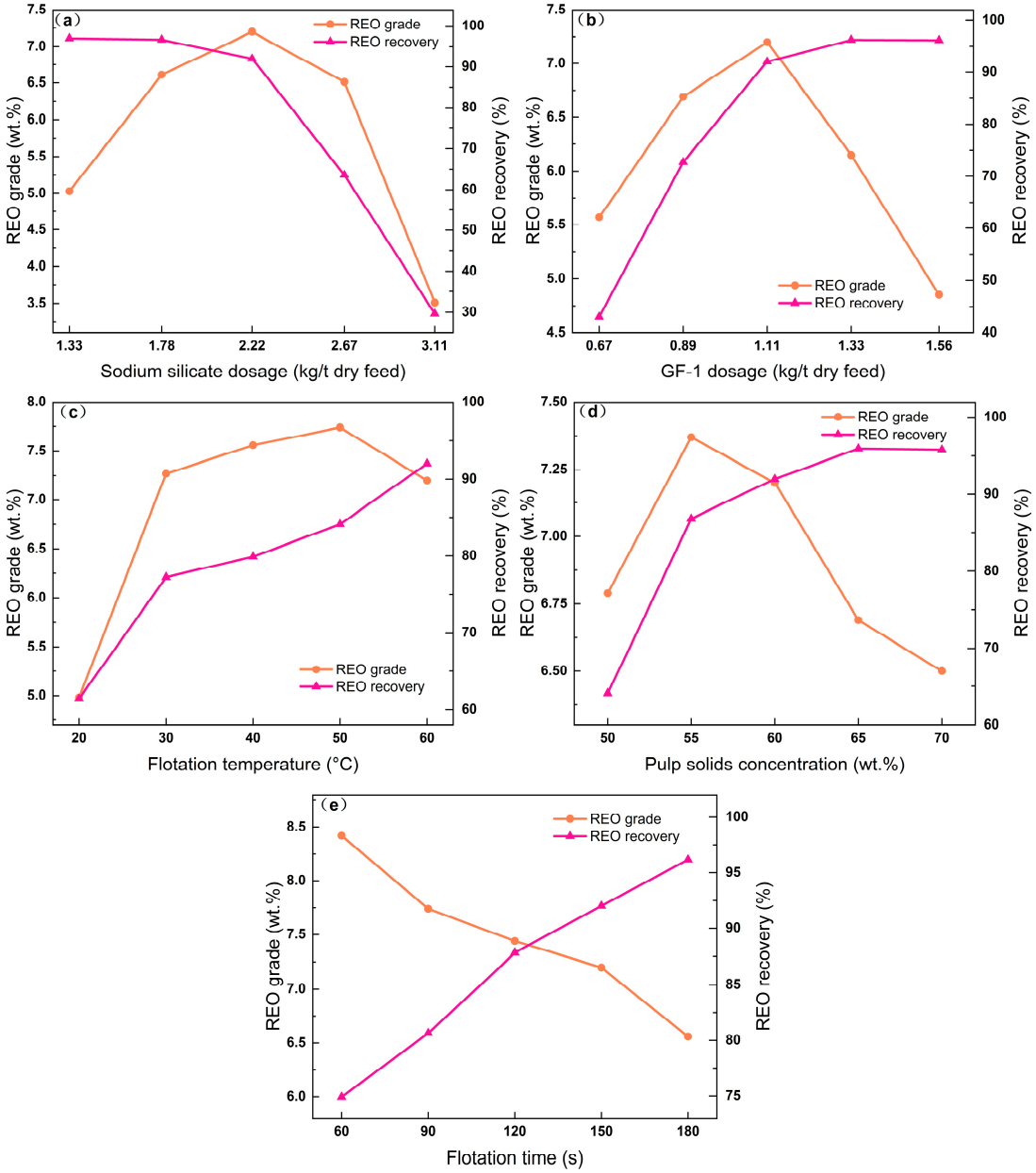


Figure 8. Effects of rougher flotation conditions on the REO grade and recovery of the concentrate: (**a**) sodium silicate dosage; (**b**) GF-1 dosage; (**c**) flotation temperature; (**d**) pulp solids concentration; and (**e**) flotation time.

Across the five replicate tests, the rougher concentrate had a mean mass yield of 23.67 ± 0.46%, an REO grade of 7.22 ± 0.11 wt.%, and a stage recovery of 92.03 ± 0.56%, whereas the rougher tailings had a mean REO grade of 0.20 wt.%. These results showed that roughing recovered most of the readily floatable rare-earth minerals. The rougher concentrate nevertheless retained substantial entrained carbonate and silicate gangue and therefore required further upgrading through multiple cleaner stages.

An open-circuit test comprising one rougher and three cleaner stages was conducted under the selected rougher flotation conditions. The results are listed in Table 7, and the corresponding mass and metallurgical balance is shown in Figure 9.

Table 6. Reproducibility test results for rare-earth rougher flotation.

Test No.	Product	Mass Yield (%)	REO Grade (wt.%)	REO Recovery (%)
1	Concentrate	23.13	7.20	92.01
	Tailings	76.87	0.19	7.99
	Feed	100	1.81	100
2	Concentrate	23.77	7.35	92.44
	Tailings	76.23	0.19	7.56
	Feed	100	1.89	100
3	Concentrate	24.02	7.32	92.06
	Tailings	75.98	0.20	7.94
	Feed	100	1.91	100
4	Concentrate	23.26	7.13	91.12
	Tailings	76.74	0.21	8.88
	Feed	100	1.82	100
5	Concentrate	24.17	7.12	92.52
	Tailings	75.83	0.19	7.48
	Feed	100	1.86	100
Mean	Concentrate	23.67 ± 0.46	7.22 ± 0.11	92.03 ± 0.56
	Tailings	76.33 ± 0.46	0.20 ± 0.01	7.97 ± 0.56
	Feed	100	1.86 ± 0.04	100

Table 7. Reproducibility test results for open-circuit rare-earth flotation.

Test No.	Product	Mass Yield (%)	REO Grade (wt.%)	REO Recovery (%)
1	Rougher tailings	76.23	0.19	7.64
	Cleaner I tailings	16.29	0.98	8.42
	Cleaner II tailings	4.11	10.35	22.41
	Cleaner III tailings	2.44	27.42	35.27
	Concentrate	0.94	53.15	26.26
	Feed	100	1.90	100
2	Rougher tailings	76.74	0.19	7.98
	Cleaner I tailings	15.97	1.05	9.18
	Cleaner II tailings	4.20	10.93	25.15
	Cleaner III tailings	2.11	26.16	30.28
	Concentrate	0.97	51.53	27.43
	Feed	100	1.83	100
3	Rougher tailings	75.98	0.19	7.70
	Cleaner I tailings	16.58	1.12	9.91
	Cleaner II tailings	4.31	10.55	24.26
	Cleaner III tailings	2.16	27.67	31.89
	Concentrate	0.98	50.41	26.24
	Feed	100	1.87	100
Mean	Rougher tailings	76.32 ± 0.39	0.19 ± 0.00	7.78 ± 0.18
	Cleaner I tailings	16.28 ± 0.31	1.05 ± 0.07	9.16 ± 0.75
	Cleaner II tailings	4.20 ± 0.10	10.61 ± 0.30	23.91 ± 1.40
	Cleaner III tailings	2.24 ± 0.18	27.08 ± 0.81	32.50 ± 2.55
	Concentrate	0.96 ± 0.02	51.70 ± 1.38	26.64 ± 0.68
	Feed	100	1.87 ± 0.04	100

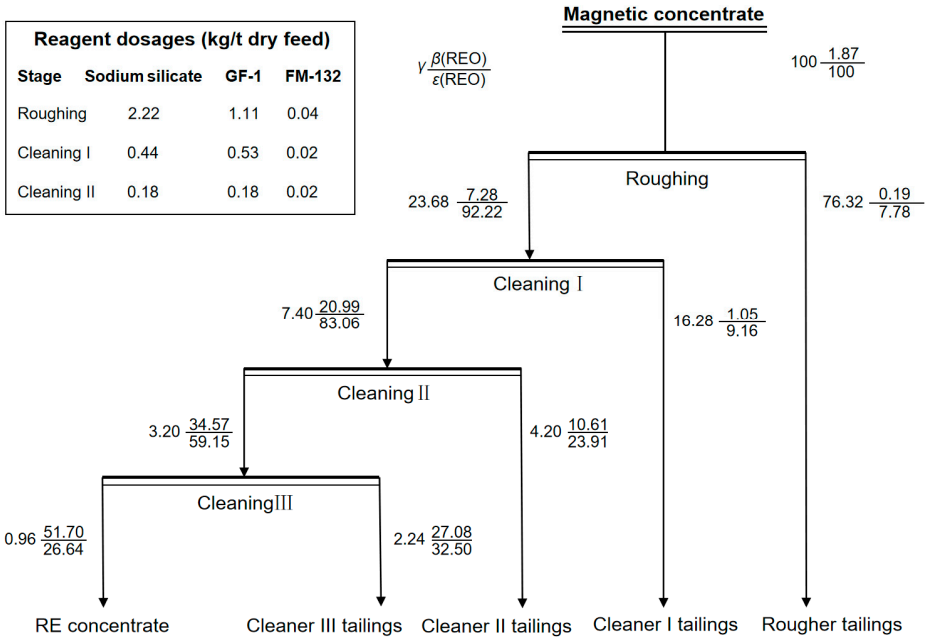


Figure 9. Mass and metallurgical balance for the open-circuit rare-earth flotation test.

Across the three open-circuit replicate tests, the final concentrate had a mean REO grade of 51.70 ± 1.38 wt.% and a mean stage recovery of 26.64 ± 0.68%. Only 26.64% of the stage REOs reported to the final concentrate. The REO grades of the Cleaner I, Cleaner II, and Cleaner III tailings increased successively. The Cleaner II and Cleaner III tailings contained 10.61 wt.% and 27.08 wt.% REOs, respectively, and together carried 56.41% of the REOs. These results showed that the cleaner middlings retained substantial rare-earth values; therefore, sequential return of middlings was required in the closed circuit to reduce rare-earth losses and increase overall recovery.

3.4. Overall Closed-Circuit Flowsheet and Characteristics of the Rare-Earth Concentrate

Based on the screening, magnetic separation, and open-circuit flotation results, a closed-circuit test comprising one rougher and three cleaner stages with sequential return of middlings was conducted to evaluate the overall flowsheet, as shown in Figure 10. The test was operated for six cycles. The mass balance and concentrate REO grade tended to stabilize during cycles 4–6; therefore, the data reported in Figure 10 are the averages of the final three cycles. Screening first rejected 32.60% of the coarse low-grade material, after which magnetic separation rejected a further 13.05% of the original feed, reducing the material entering flotation to 54.35% of the original feed mass, increasing the REO grade from 1.32 wt.% to 1.82 wt.%, and retaining 74.94% of the REOs in the original feed. Closed-circuit flotation with one rougher and three cleaner stages ultimately produced a rare-earth concentrate containing 51.99 wt.% REOs at an overall recovery of 52.38%, corresponding to an enrichment ratio of 39.4 relative to the original feed. These results indicate that screening and magnetic separation achieved selective feed mass reduction and preconcentration at the front end, while the sequential middlings return provided additional separation opportunities for fine rare-earth minerals and intergrowths during cleaning, ultimately enabling the production of a high-grade rare-earth concentrate.

The overall REO recovery was 52.38%, and the recovery loss resulted mainly from cumulative REO losses across the individual stages. In descending order of loss, 17.96% of the REOs were lost in the final tailings discharged from the cleaning circuit, 16.26% in the screening coarse tailings, 8.80% in the magnetic separation tailings, and 4.60% in the rougher tailings. The largest loss occurred in the cleaning circuit tailings, indicating that some

fine rare-earth minerals and rare-earth–gangue intergrowths remained unrecovered after multiple cleaning stages. Future improvement should therefore prioritize the regrinding and retreatment of REO-rich cleaner tailings, the introduction of a scavenging stage, or optimization of middlings return to increase liberation and recovery opportunities for intergrowths. The second-largest loss occurred in the screening coarse tailings; regrinding and retreating the +74 μm fraction could reduce rare-earth losses caused by direct rejection of coarse intergrowths. For the magnetic separation tailings, further optimization of the magnetic flux density, feed velocity, and pulp solids concentration, or the addition of a second magnetic -separation stage, could reduce rare-earth losses. Rougher tailings losses were comparatively low and could be further reduced by optimizing the collector dosage, flotation time, and pulp conditions. Accordingly, future efforts to increase overall recovery should focus primarily on rare-earth losses in the cleaning tailings and screening coarse fraction.

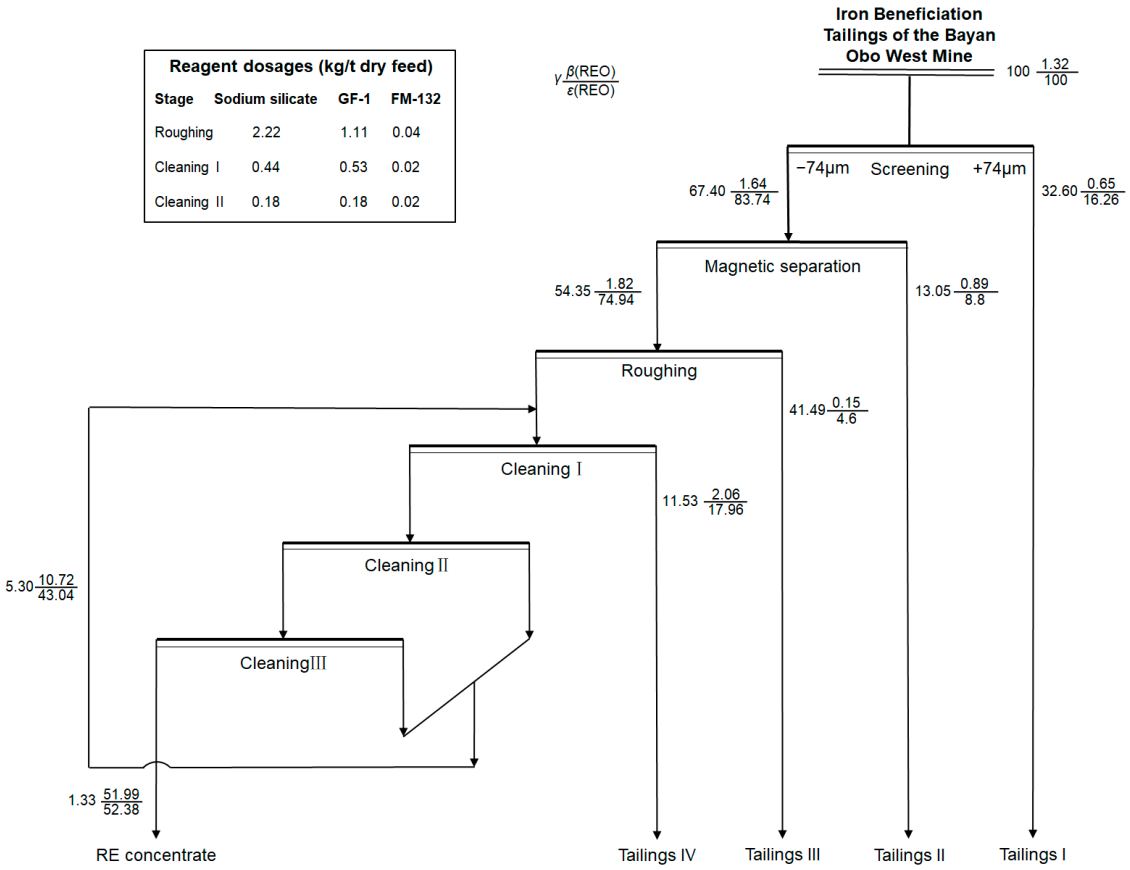


Figure 10. Mass and metallurgical balance for the overall flowsheet comprising screening, magnetic separation, and closed-circuit flotation with one rougher and three cleaner stages for the West Mine iron beneficiation tailings.

The XRD pattern in Figure 11 shows that the principal diffraction peaks were assigned to bastnäsite and monazite, whereas only minor peaks corresponded to dolomite and apatite. This indicates that the target rare-earth minerals had become the dominant crystalline phases and that the diffraction intensities of gangue minerals were substantially reduced. Figure 12 presents the mineralogical characterization of the flotation concentrate and shows the transformation from a feed dominated by carbonate and silicate gangue to a concentrate dominated by rare-earth minerals. Figure 12a presents the AMICS map of all mineral phases, with colors corresponding to the minerals listed in the legends of Figure 12c,d. In the feed map in Figure 2a, dolomite, mica, amphibole, and other gangue minerals occupied

much of the field of view. In contrast, the concentrate map in Figure 12a contained a markedly higher abundance and denser distribution of monazite and bastnäsite, with only small amounts of dolomite, apatite, and other gangue remaining. This contrast showed that screening, magnetic separation, and closed-circuit flotation selectively concentrated the target rare-earth minerals. Figure 12b isolates bastnäsite, monazite, parisite-(Ce), and the other rare-earth phases from the complete mineral classification. Their distribution was denser and more continuous than the sparse, spot-like distribution in the feed map in Figure 2b, consistent with the enrichment of monazite and bastnäsite in the final concentrate. The quantitative results in Figure 12c showed that rare-earth minerals accounted for 82.55 wt.% of the concentrate, while dolomite and apatite accounted for 5.51 wt.% and 3.79 wt.%, respectively, and the remaining minerals occurred at low contents. By comparison, the feed contained 37.58 wt.% dolomite, 15.55 wt.% mica, and only 2.07 wt.% total rare-earth minerals. The principal carbonate and silicate gangue minerals were therefore substantially depleted, while the rare-earth minerals were strongly enriched. Figure 12d further showed that monazite and bastnäsite accounted for 41.65 wt.% and 33.96 wt.% of the concentrate, respectively, and parisite-(Ce) accounted for 5.21 wt.%. The remaining rare-earth minerals were present at low levels. The higher monazite content relative to bastnäsite was consistent with the greater contribution of monazite to the total REOs in the feed and its higher degree of liberation. The concentrate nevertheless retained 5.51 wt.% dolomite and 3.79 wt.% apatite because of mineral intergrowths, similar surface chemical properties, and mechanical entrainment of ultrafine particles. This residual gangue was consistent with the complex mineral associations shown in Figure 4 and Table 4. Thus, although the closed circuit produced a concentrate containing 51.99 wt.% REOs, overall recovery remained constrained by fine intergrowths and by the efficiency with which particles were recovered during cleaner middlings recirculation.

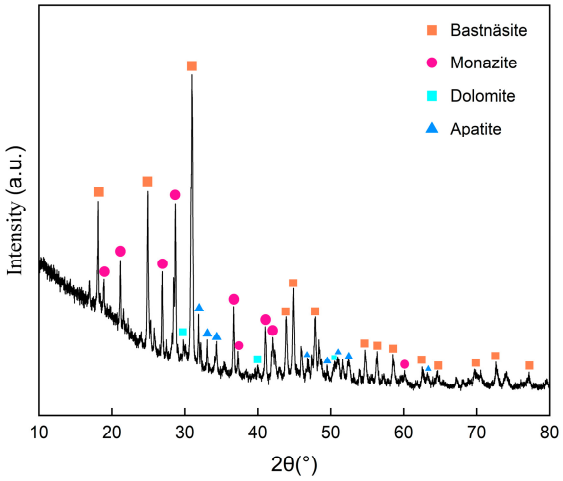


Figure 11. XRD pattern of the rare-earth concentrate.

The overall flowsheet assigned distinct functions to upstream selective feed mass reduction, intermediate magnetic preconcentration, and downstream intensive flotation upgrading. Screening and magnetic separation jointly rejected 45.65% of the material, reducing the flotation feed to 54.35% of the original feed mass. For a fixed amount of original feed, this mass reduction would decrease the solids load entering the flotation circuit, the required flotation cell volume, the energy demand for pulp heating and agitation, and the total consumption of depressant, collector, and frother. Sequential middlings recycling provided additional separation opportunities for fine rare-earth minerals and intergrowths that might otherwise be lost during cleaning and prevented REO-rich middlings from being discharged directly to the tailings. The final concentrate contained 51.99 wt.% REOs

at an overall recovery of 52.38%. The results demonstrate that screening-based feed mass reduction, magnetic preconcentration, and closed-circuit flotation can produce a high-grade rare-earth concentrate from the Bayan Obo West Mine iron beneficiation tailings while reducing the flotation load. The flowsheet provides a basis for subsequent continuous testing, flowsheet optimization, and scale-up validation; further application should be verified using samples from different production periods and should evaluate continuous operation stability, pulp-heating energy demand, reagent consumption, and economics.

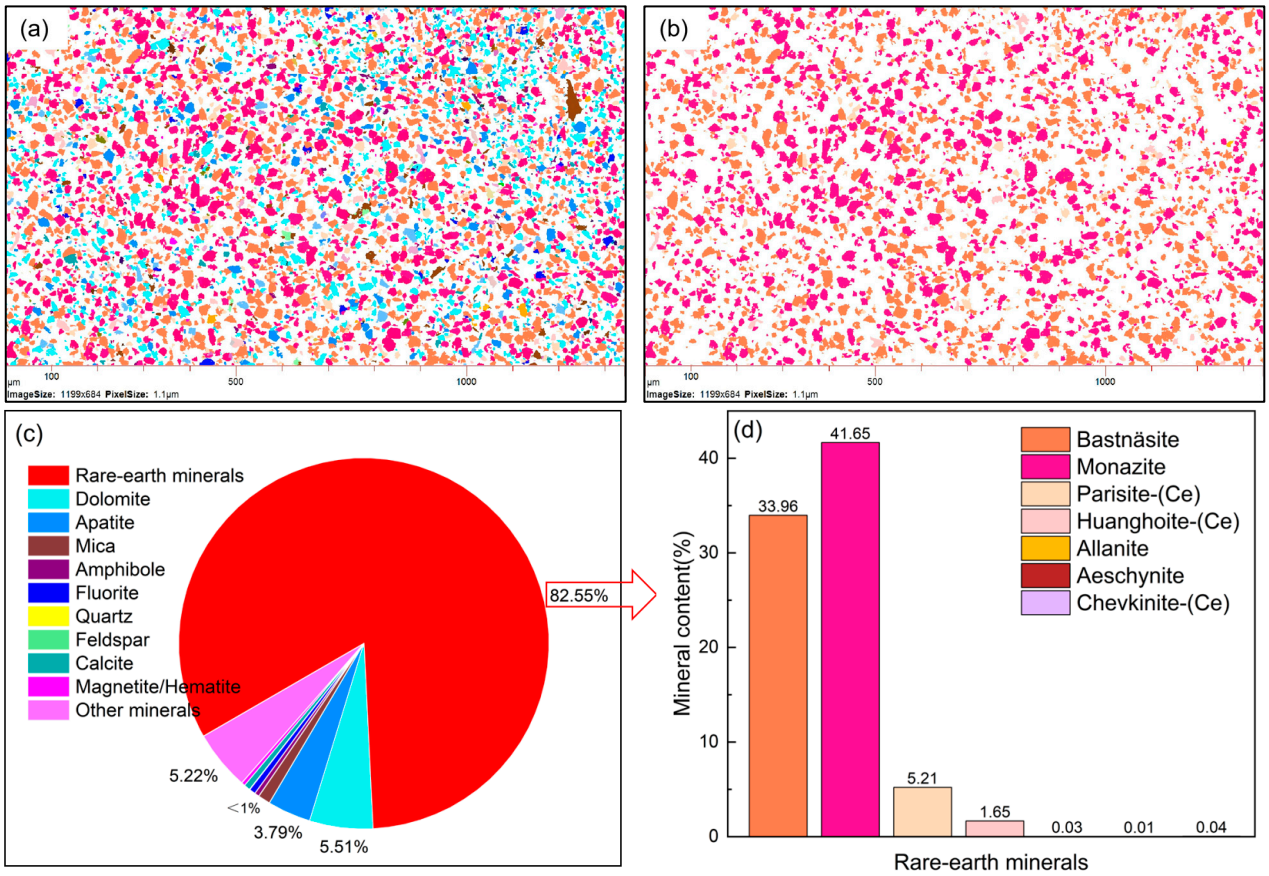


Figure 12. Mineralogical characterization of the closed-circuit rare-earth flotation concentrate: (**a**) AMICS mineral map of all phases; (**b**) AMICS rare-earth mineral map; (**c**) major mineral composition; and (**d**) rare-earth mineral composition.

4. Conclusions

By integrating detailed mineralogical characterization with screening, magnetic separation, and closed-circuit flotation tests comprising one rougher and three cleaner stages, this study evaluated the recovery of rare-earth minerals from the low-grade, fine-grained iron beneficiation tailings of the Bayan Obo West Mine characterized by complex mineral intergrowths. The principal conclusions are as follows:

(1) The West Mine iron beneficiation tailings contained 1.32 wt.% REOs and represented a low-grade secondary rare-earth resource. Monazite and bastnäsite hosted 47.39% and 39.19% of the total REOs, respectively, together accounting for 86.58%, and the −25 μm fraction contained 49.74% of the total REOs. The degrees of liberation of monazite and bastnäsite were 65.09% and 48.43%, respectively, while bastnäsite was associated with carbonate minerals, silicate minerals, and fluorite at proportions of 24.07%, 10.01%, and 7.42%, respectively. Thus, the low feed grade, preferential enrichment of rare earths in the fine fractions, incomplete liberation of rare-earth minerals, and multiphase intergrowths

with carbonates, silicates, fluorite, apatite, and iron-bearing minerals were the principal mineralogical factors limiting efficient rare-earth recovery from the tailings.

(2) Based on the particle size–grade relationship, screening at 74 μm rejected a coarse low-grade fraction with a mass yield of 32.60% and an REO grade of 0.65 wt.%, while increasing the REO grade of the −74 μm undersize to 1.64 wt.%. Subsequent wet high-intensity magnetic separation further rejected low-magnetic-response gangue, so that the magnetic concentrate entering flotation represented only 54.35% of the original feed mass, contained 1.82 wt.% REOs, and retained 74.94% of the REOs in the original feed. Screening and magnetic separation together reduced the solids load on downstream flotation by 45.65%, demonstrating that the principal value of preconcentration was selective feed mass reduction while maintaining a relatively high REO retention, rather than the pursuit of a high enrichment ratio in the preconcentration stage alone.

(3) Under the reagent system used in this study, the selected rougher flotation conditions were 2.22 kg/t sodium silicate, 1.11 kg/t GF-1, 0.04 kg/t FM-132, a pulp solids concentration of 60 wt.%, a temperature of 60 °C, and a flotation time of 150 s, under which the rougher REO stage recovery was 92.03 ± 0.56%. Closed-circuit flotation with one rougher and three cleaner stages and sequential return of middlings ultimately produced a rare-earth concentrate containing 51.99 wt.% REOs at an overall recovery of 52.38% relative to the original feed, corresponding to an enrichment ratio of 39.4. Rare-earth minerals accounted for 82.55 wt.% of the concentrate, including 41.65 wt.% monazite, 33.96 wt.% bastnäsite, and 5.21 wt.% parisite-(Ce); the principal gangue minerals were substantially depleted.

(4) Overall, this study demonstrated the feasibility of applying the integrated screening–magnetic separation–one-rougher/three-cleaner closed-circuit flotation flowsheet to the preconcentration and recovery of rare earths from the Bayan Obo West Mine iron beneficiation tailings. The overall REO loss was 47.62%, with the principal losses occurring in the final cleaning circuit tailings and screening coarse tailings, at 17.96% and 16.26%, respectively; REO losses in the magnetic separation tailings and rougher tailings were lower, at 8.80% and 4.60%, respectively. Therefore, future improvements in overall rare-earth recovery should focus on losses in the coarse fraction and cleaning tailings. For a 500 kg batch of original feed containing 1.32 wt.% REOs, the feed would contain approximately 6.60 kg REOs. At an overall recovery of 52.38% and a concentrate grade of 51.99 wt.% REOs, approximately 6.65 kg of rare-earth concentrate would be obtained, containing about 3.46 kg REOs and corresponding to a concentrate mass yield of approximately 1.33%.

Author Contributions: Conceptualization, Y.J. (Yongli Jin) and Y.J. (Yan Jia); methodology, X.W., Y.J. (Yongli Jin) and Y.J. (Yan Jia); validation, X.W. and Y.J. (Yan Jia); formal analysis, X.W.; investigation, X.W., Y.W. and C.D.; resources, Y.L.; data curation, X.W.; writing—original draft preparation, X.W.; writing—review and editing, Y.J. (Yongli Jin) and Y.J. (Yan Jia); visualization, X.W.; supervision, Y.J. (Yongli Jin) and Y.J. (Yan Jia); project administration, Y.J. (Yongli Jin); funding acquisition, Y.J. (Yongli Jin). All authors have read and agreed to the published version of the manuscript.

Funding: This research was funded by the Project of the Department of Education of Inner Mongolia Autonomous Region (YLXKZX-NKD-041), the Program of the Department of Science and Technology of Inner Mongolia Autonomous Region (2025YFHH0049, 2025KYPT0129), and the Project of the State Key Laboratory of Bayan Obo Rare Earth Resource Researches and Comprehensive Utilization (NKDHX2025032/2025QZ2656).

Data Availability Statement: The data presented in this study are available within the article. Further inquiries may be directed to the corresponding author.

Acknowledgments: The authors gratefully acknowledge the support of the Project of the Department of Education of Inner Mongolia Autonomous Region (YLXKZX-NKD-041), the Program of the

Department of Science and Technology of Inner Mongolia Autonomous Region (2025YFHH0049, 2025KYPT0129), and the Project of the State Key Laboratory of Bayan Obo Rare Earth Resource Researches and Comprehensive Utilization (NKDHX2025032/2025QZ2656). The authors also thank the National and Local Joint Engineering Research Center of Comprehensive Utilization of Wastes from Mining, Beneficiation, and Smelting of Bayan Obo Associated and Co-occurring Ores, the Carbon Neutrality Engineering Research Center of Colleges and Universities in Inner Mongolia Autonomous Region, and the State Key Laboratory of Bayan Obo Rare Earth Resource Researches and Comprehensive Utilization for providing experimental and analytical support. During the preparation of the Graphical Abstract for this manuscript, the authors used ChatGPT (OpenAI, accessed in August 2026) to assist with the visualization and graphical presentation of the authors' original research content. The authors have reviewed and edited the output and take full responsibility for the content of this publication.

Conflicts of Interest: The authors declare no conflicts of interest.

References

1. Kim, J.; Choi, J.; Lee, S. A Review of Rare Earth Elements Recovery from Bastnaesite Ore: From Beneficiation to Metallurgical Processing. *J. Sustain. Metall.* **2025**, *11*, 773–798. [CrossRef]
2. Shuai, Z.; Zhu, Y.; Gao, P.; Han, Y. Rare Earth Elements Resources and Beneficiation: A Review. *Miner. Eng.* **2024**, *218*, 109011. [CrossRef]
3. Cheng, S.; Li, W.; Han, Y.; Sun, Y.; Gao, P.; Zhang, X. Recent Process Developments in Beneficiation and Metallurgy of Rare Earths: A Review. *J. Rare Earths* **2024**, *42*, 629–642. [CrossRef]
4. Julapong, P.; Numprasanthai, A.; Tangwattananukul, L.; Juntarasakul, O.; Srichonphaisarn, P.; Aikawa, K.; Park, I.; Ito, M.; Tabelin, C.B.; Phengsaart, T. Rare Earth Elements Recovery from Primary and Secondary Resources Using Flotation: A Systematic Review. *Appl. Sci.* **2023**, *13*, 8364. [CrossRef]
5. Yang, L.; Yan, G.Y.; Yang, B.; Meng, W.X.; Liu, J.Y.; Yu, J.F. *Minerals of Bayan Obo Deposit*; Geological Publishing House: Beijing, China, 2024.
6. Shao, D.; Du, X.; Deng, Y.; Yan, Z.; Duan, W.; Yu, H.; Qi, T. The Process Mineralogical Characterization of Bayan Obo Rare-Earth Tailings and Density Functional Theory Study of the Occurrence State of Sc. *Minerals* **2023**, *13*, 1287. [CrossRef]
7. Chen, Y.; He, D.; Potgieter, J.H. Development and Beneficiation Technology of Rare Earth Ores in China. *J. South. Afr. Inst. Min. Metall.* **2022**, *122*, 125–132. [CrossRef]
8. Silva, C.M.; Lode, S.; Aasly, K.; Kowalczuk, P.B. Early-Stage Application of Process Mineralogy Methodologies for Mineral Tracking in Flotation of Rare Earth Elements (REE)-Bearing Minerals from a Deposit in Norway. *Miner. Eng.* **2023**, *202*, 108268. [CrossRef]
9. Park, I.; Kanazawa, Y.; Sato, N.; Galtchandmani, P.; Jha, M.K.; Tabelin, C.B.; Jeon, S.; Ito, M.; Hiroyoshi, N. Beneficiation of Low-Grade Rare Earth Ore from Khalzan Buregtei Deposit (Mongolia) by Magnetic Separation. *Minerals* **2021**, *11*, 1432. [CrossRef]
10. Xiong, W.L.; Deng, J.; Chen, B.Y.; Deng, S.Z.; Wei, D.Z. Flotation-Magnetic Separation for the Beneficiation of Rare Earth Ores. *Miner. Eng.* **2018**, *119*, 49–56. [CrossRef]
11. Wang, W.; Li, E.; Li, Z.; Zhu, W.; Wang, Y. Recovery of Xenotime and Florencite from Silicate Minerals Using a Combined Technique of Magnetic Separation and Flotation. *Minerals* **2024**, *14*, 1073. [CrossRef]
12. Abaka-Wood, G.B.; Johnson, B.; Addai-Mensah, J.; Skinner, W. Recovery of Rare Earth Elements Minerals in Complex Low-Grade Saprolite Ore by Froth Flotation. *Minerals* **2022**, *12*, 1138. [CrossRef]
13. Sauber, M.E.; Di Feo, A.; Almusned, B.; Hart, B. Improved Monazite Flotation through Combined Use of Oleic Acid and Alkyl Hydroxamate: A Surface Chemistry Approach. *Miner. Eng.* **2025**, *228*, 109368. [CrossRef]
14. Qin, Y.F.; Li, N.; Ma, Y.; Wang, Q.W. Experimental Study on Preferential Flotation of Rare Earths from Iron Ore Processing Tailings in Baiyun Ebo. *Min. Metall.* **2021**, *30*, 32–37. [CrossRef]
15. Wang, L.M.; Li, H.J.; Bai, C.X.; Sui, Y.T.; Liu, T. Experimental Study on Comprehensive Recovery of Rare Earth and Fluorite from an Iron Tailings of Concentrator in Bayan Obo. *Conserv. Util. Miner. Resour.* **2022**, *42*, 52–59. [CrossRef]
16. Fan, H.L.; Wang, J.Y.; Qu, Q.L.; Liu, M.B. Separation of Rare Earth Minerals from Bayan Obo Ore by Direct Flotation Process. *Chin. Rare Earths* **2017**, *38*, 76–84.
17. Wang, J.L.; Sun, H.T.; Zhao, Z.W.; Ren, H.; Lei, X. Enrichment Behavior of Weak Magnetic Rare Earth and Niobium in Bayan Obo Ore through Cascade Magnetic Separation. *J. Chin. Soc. Rare Earths* **2025**, *43*, 205–214.
18. Zhang, M.; Chen, F.; Yan, G.; Li, H.; Li, J.; Peng, G.; Yu, H. The Distribution Regularity and Flotation Study of Niobium-Bearing Minerals in Baiyun Obo. *Minerals* **2023**, *13*, 387. [CrossRef]

19. Tang, S.Y.; Li, Y.X. Experimental Study on Mineral Processing of Iron Bearing Rocks in Bayan Obo West Mine. *China Min. Mag.* **2024**, *33*, 226–234. [CrossRef]
20. Cao, Y.; Liu, D. Study on Process Mineralogy and Rare Earth, Fluorite Flotation Test of West Mine in Bayan Obo. *Min. Metall.* **2023**, *32*, 55–63. [CrossRef]
21. Zhao, N.; Zhang, Q.; Ma, H.; Sun, Y.; Gao, P.; Cao, Z.; Zhang, Z. Advancing the Recovery of Iron and Rare Earth Elements from the Solid Waste at Bayan Obo. *Int. J. Min. Sci. Technol.* **2025**, *35*, 295–306. [CrossRef]
22. Wang, J.; Cheng, Z.; Hu, Y.; Cao, Y.; Wang, P.; Cao, Z. Depression Behavior and Mechanism of Sodium Silicate on Bastnaesite and Parisite Flotation. *Colloids Surf. A Physicochem. Eng. Asp.* **2021**, *631*, 127691. [CrossRef]
23. Cao, Z.; Cheng, Z.; Wang, J.; Cao, Y. Synergistic Depression Mechanism of Ca^{2+} Ions and Sodium Silicate on Bastnaesite Flotation. *J. Rare Earths* **2022**, *40*, 988–995. [CrossRef]
24. Chapleski, R.C., Jr.; Chowdhury, A.U.; Wanhala, A.K.; Gibson, L.D.; Stamberga, D.N.; Jansone-Popova, S.; Sacci, R.L.; Meyer, H.M., III; Stack, A.G.; Bocharova, V.; et al. Improving Rare-Earth Mineral Separation with Insights from Molecular Recognition: Functionalized Hydroxamic Acid Adsorption onto Bastnäsite and Calcite. *Langmuir* **2022**, *38*, 5439–5453. [CrossRef]
25. Boulanger, J.-F.; Bazin, C.; Turgeon, K. Effect of Depressants and Temperature on Bastnaesite and Monazite Flotation Separation from a Canadian Rare Earth Element (REE) Ore. *Minerals* **2019**, *9*, 225. [CrossRef]
26. Wang, L.; Runge, K.; Peng, Y. The Observed Effect of Flotation Operating Conditions and Particle Properties on Water Recovery at Laboratory Scale. *Miner. Eng.* **2016**, *94*, 83–93. [CrossRef]
27. Hoang, D.H.; Heitkam, S.; Kupka, N.; Hassanzadeh, A.; Peuker, U.A.; Rudolph, M. Froth Properties and Entrainment in Lab-Scale Flotation: A Case of Carbonaceous Sedimentary Phosphate Ore. *Chem. Eng. Res. Des.* **2019**, *142*, 100–110. [CrossRef]

Disclaimer/Publisher's Note: The statements, opinions and data contained in all publications are solely those of the individual author(s) and contributor(s) and not of MDPI and/or the editor(s). MDPI and/or the editor(s) disclaim responsibility for any injury to people or property resulting from any ideas, methods, instructions or products referred to in the content.